The British Dam Society

Lessons for dam safety in the UK from the landslide-generated waves incident in the Apporo dam reservoir, Japan

M HEIDARZADEH, University of Bath
V HELLER, University of Nottingham
T ZHAO, Brunel University London
C GOFF, HR Wallingford

SYNOPSIS We report and analyse the damage caused by landslide-generated waves in the Apporo reservoir (Japan) and take lessons for dam safety in the UK. The incident occurred in September 2018 following an M6.6 earthquake and typhoon Jebi. Apporo dam is a trapezoidal Cemented Sand and Gravel dam with a height of 47.2m. The simultaneous occurrence of the earthquake and the typhoon triggered thousands of landslides. Through field surveys, we identified several landslides on the banks of the reservoir at a close distance to the dam, causing a runup height of 5.3m at the shore. Visible damage, confirmed by site engineers, indicated that the waves damaged the reservoir bank revetments. Here, we model the landslide using Plaxis 3D, replicate the landslide-generated waves applying empirical equations, and discuss the lessons for dam safety in the UK. Using GIS data on elevation, rainfall, and seismicity, we identified the UK regions most susceptible to landslides. Region 3, the highest risk area, contains 252 large reservoirs, indicating the need to include landslide-generated wave risks in assessments of potential failure modes. We discuss prediction capabilities that can be applied for hazard and risk assessment of UK reservoirs regarding landslide-generated waves and propose a four-step methodology for such assessments.

INTRODUCTION AND BACKGROUND

Landslide-generated waves were reported at the Apporo dam reservoir (Hokkaido, Japan) on 5th September 2018 (UTC) following a magnitude (M) 6.6 earthquake and the passage of the Super-Typhoon Jebi (Figure 1). Due to the almost concurrent occurrences of the earthquake and the typhoon, thousands of landslides were generated in the region leading to significant damage to properties and infrastructure and killing 36 people (Yamagishi and Yamazaki 2018; Zhang et al. 2019). According to various reports, nearly 6,000 landslides were generated in the region (e.g. Aimaiti et al. 2019; Zhang et al. 2019), some of which occurred in the Apporo dam reservoir and caused damage (Figure 1) (Heidarzadeh et al. 2023). The field surveys conducted by the authors confirmed the damage from landslide-generated waves; however, the damage was limited and did not threaten the dam's safety.

Landslide-generated waves in reservoirs are considered as major threats for dam safety worldwide. Heller and Ruffini (2023) identified 33 past landslide-generated waves, due to both subaerial and partially submerged landslides, which resulted in a cumulative death toll

in excess of 58,000 due to the waves combined with associated phenomena such as volcanic explosions and landslides. Some of them occurred in reservoirs including the catastrophic Vajont reservoir event in 1963 in Italy where a 240 million m^3 of soil mass on the left valley flank became unstable. The generated wave overtopped the 262m tall arch dam by approximately 70m and destroyed the village of Longarone killing about 2,000 people (Müller 1964). A number of landslide-generated waves were repeatedly observed in the Three Gorges Reservoir in China in 2003 (Qianjiangping, Yin et al. 2015), 2008 (Gongjiafang, Huang et al. 2012) and 2015 (Hongyanzi, Xiao et al. 2018). Although generated far away from the dam, these waves resulted in severe damage in the proximity of the slide impact by reaching runup heights of up to 39m and killing people in both 2003 and 2015 events.

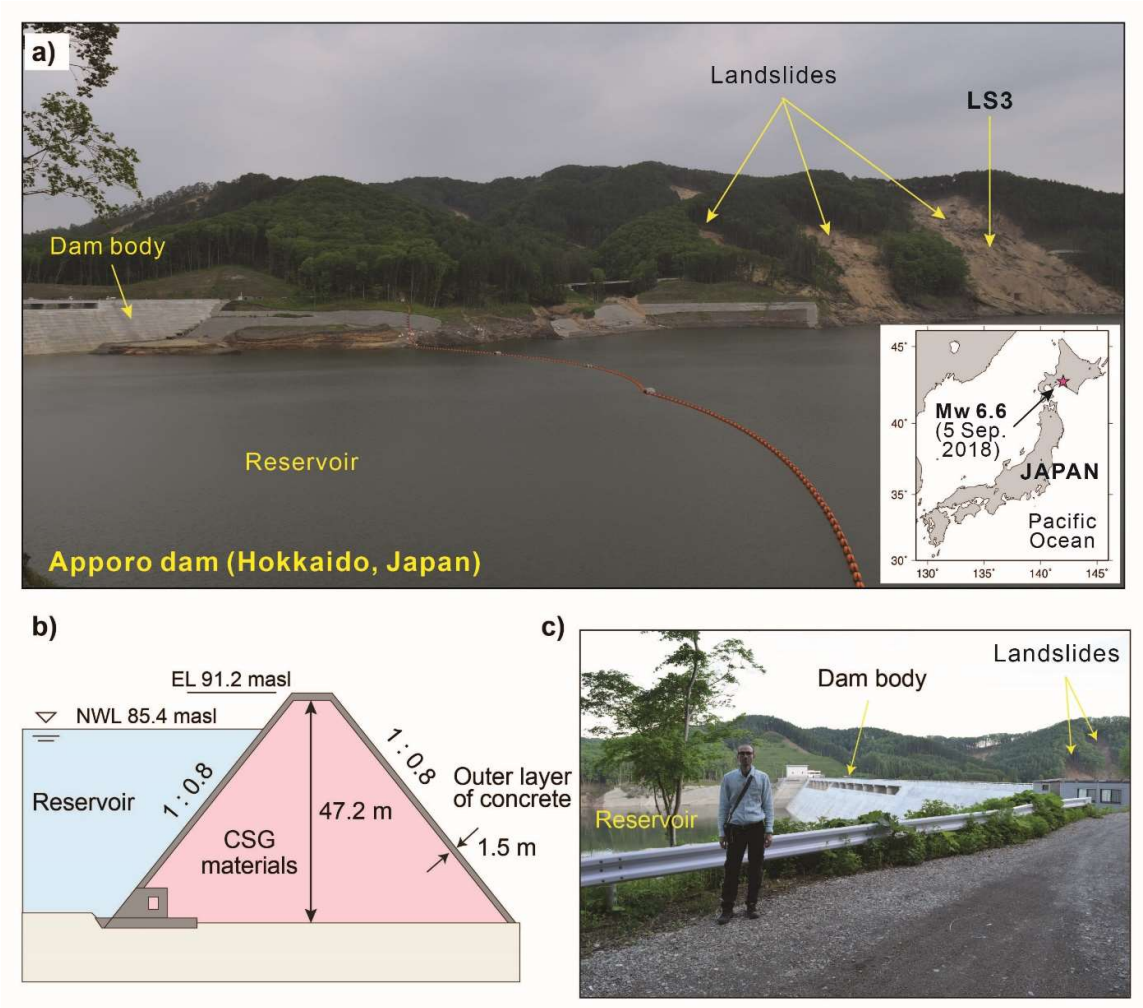

Figure 1. a): Location of the dam and the landslides due to the 5th September 2018 M6.6 earthquake. **b):** A sketch of the dam body cross section. **c):** A photo showing the dam, the reservoir and a few co-seismic landslides. NWL and masl are abbreviations for "Normal Water Level", and "metres above sea level", respectively.

The Clyde reservoir in New Zealand is a rare example where a creeping mass could be stopped (MacFarlane and Jenks 1996). Huang et al. (2023) suggested to remove parts of the WangJiaShan landslide in the Baihetan reservoir in China to reduce the wave risk. Other measures to minimise damage are evacuation of the population, reservoir drawdown,

controlled slide blasting and, when designing the dam, provision of adequate freeboard or adding a wave protection wall on the dam crest (Evers et al. 2019). An extreme measure would be partial removal of the dam.

Empirical equations help in the preliminary determination of the risks associated with a threatening landslide. Such empirical equations can be derived from laboratory experiments under systematic variation of the governing parameters under idealised conditions. The generic empirical equations express the wave parameters in functions of these governing parameters (Heller and Ruffini 2023). Figure 2 shows the relevant slide and wave parameters during wave generation, propagation and runup. The governing parameters are the bulk slide volume $\forall_s$, slide density ρ_s, slide thickness s, slide width b_s, slide impact velocity V_s, slope angle α, and still water depth h. These parameters can be expressed dimensionless as the slide Froude number $F = V_s/(gh)^{1/2}$, the relative slide thickness $S = s/h$ and the relative slide mass $M = \forall_s\rho_s/(\rho_w b_s h^2)$ where g is the gravitational acceleration, and ρ_w the water density. In the approach from Evers et al. (2019), applied herein, these parameters are merged into the impulse product parameter $P = FS^{1/2}M^{1/4}\{\cos[(6/7)\alpha]\}^{1/2}$ (Heller and Hager 2010). Important wave parameters are the maximum wave amplitude a_M and height H_M as well as their evolutions $a(r, \gamma)$ and $H(r, \gamma)$ with the radial distance r and wave propagation angle γ. The wave runup at a dam or shore is characterised with the runup height R and the potential overtopping volume $\forall$ depending on h in front of the dam or shore, the runup angle β, the freeboard f and the dam crest width b_K (Figure 2).

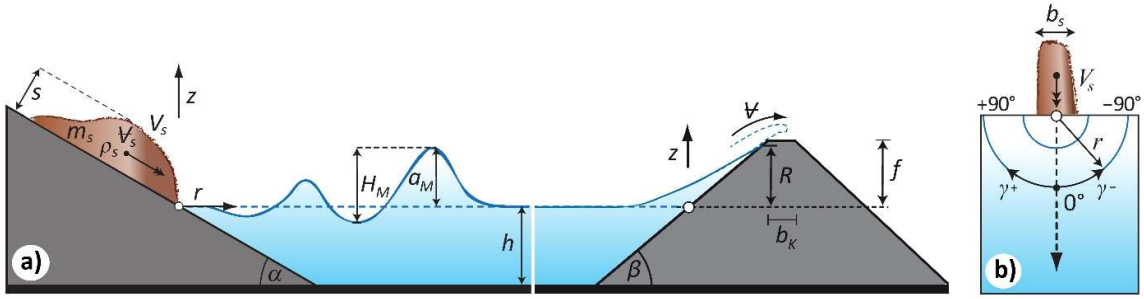

Figure 2. Definition sketches showing **a):** A side view of the slide, landslide-generated waves propagation and runup at an embankment dam, and **b):** A plan view of the slide and wave propagation in an idealised reservoir.

In the UK, the safety of dams is controlled by well-established laws, which are the Reservoirs Act 1975 in England and Wales (Acford 2015), and the Reservoirs (Scotland) Act 2011 in Scotland (Macdonald 2011). Under this legislation, panels of specialist engineers carry out regular Supervising Engineer inspections at least annually, and additional independent Inspecting Engineer inspections are carried out at least every 10 years. Guidance to these engineers suggests consideration of the reservoir rim stability, but it is not common or practical for the Engineer to walk the entire reservoir rim or to undertake geotechnical investigations. Other than comments on changes of land use from recent maps, or obvious slips visible from the dam, there is currently no standard analysis that can be carried out to assess the susceptibility of the reservoir to a landslide induced wave.

The purpose of this paper is to report the findings of the field surveys conducted by the authors following the landslide-generated waves incident in the Apporo dam reservoir, to supplement the surveys with modelling efforts and to take lessons for dam safety in the UK.

We also present prediction capabilities applicable for hazard and risk assessment of UK reservoirs concerning landslide-generated waves, and propose a four-step methodology.

CHARACTERISTICS OF THE DAM AND RESERVOIR

Japan has a large portfolio of dams and is considered one of the most active countries in terms of dam construction worldwide. There are over 2,200 large dams (height more than 15 m) in Japan, the majority of which are constructed for irrigation purposes (Itsukushima 2022; Sasaki and Kondo 2018). The Apporo dam, with a height of 47.2m and a crest length of 516m (Figure 1b,c), is constructed using the cemented sand and gravel (CSG) technology which is a relatively new technology developed in Japan for dam construction. According to the Japan Commission on Large Dams (2018), there are several benefits for constructing dams using the CSG technology, including: smaller carbon emissions, higher stabilities for the dam, and lower maintenance costs. A cross section of the dam is shown in Figure 1b where a 1.5m concrete layer is seen as the top protective layer of the dam body. The capacity of the reservoir is approximately 47 million m3 of water.

DATA AND METHODS

The methodology employed in this research is a combination of field surveys, modelling of maximum wave amplitudes based on empirical equations, and numerical modelling of slope failures. Field surveys were conducted in the period from 29 May to 4 June 2019 to collect data on the landside sizes, locations, and the wave runup heights. The landslide and the damage from the waves were surveyed, photographed, and their information were recorded with the aid of a TruPulse 200 laser rangefinder.

For modelling maximum wave amplitudes of subaerial landslide-generated waves, a wide range of empirical equations is available (Heidarzadeh et al. 2023; Heller and Ruffini 2023). The manual developed by Evers et al. (2019) has been commissioned by the Swiss Federal Office of Energy, responsible for dam safety in Switzerland. In contrast to other approaches, this manual consists of a collection of empirical equations centred around the impulse product parameter P to holistically predict the effects of landslide-generated waves in lakes and reservoirs including wave runups, overland flows, dam overtopping volumes, and flow depths as well as forces on dams. This manual is used here with the aim to predict the observed runup height R at the shore and also a value at the dam. Evers et al. (2019), and the previous version in Heller et al. (2009), have been applied for preliminary hazard assessments in a number of locations including in Austria (Gabl et al. 2015), the Himalaya (Sattar et al. 2021), Switzerland (Fuchs and Boes 2010) and Turkey (Ersoy et al. 2019). As the waves in the Apporo lake propagate freely on semi-circles, the 3D approach in Evers et al. (2019) is most suitable.

The Finite Element Method (FEM) numerical package Plaxis 3D has been used in this research to solve the full hydro-mechanical coupling between soil deformations, consolidation and groundwater flow simultaneously using the Biot's theory (Biot 1956). The theory assumes the soil consolidation is driven by the evolution of excess pore water pressure within the solid element. The soil deformation (e.g., displacement and strain fields) is solved by FEM, while the fluid flow analysis uses the Finite Difference Method (FDM) to solve the pore water pressure field. This approach is critically important in the context of slope stability analysis because the slope deformation is affected by the changes of pore water pressure, and thus the changes in effective stress. The Hardening Soil model with small-strain stiffness (HS-Small model) was used to characterise the behaviour of the topsoil (~up to 3m below the ground

surface), while the classical Mohr-Coulomb model was employed for the deeper ground. The HS-Small model will show typical hysteretic behaviour under the earthquake cyclic shear loading. The ground movement earthquake signals were first processed by applying the baseline correction and then applied at the base of the model. The bottom of the model has a fixed compliant base boundary condition, while other boundaries have a normally fixed free-field condition.

The data regarding earthquake mainshock and one-month aftershocks were provided by the United States Geological Survey (USGS) earthquake catalogue: (https://earthquake.usgs.gov/earthquakes/search/).

Typhoon data were downloaded from the ZOOM EARTH weather data: (https://zoom.earth/storms/jebi-2018/#map=satellite-hd).

Data regarding reservoir water level and volume before and after the earthquake were supplied by the Hokkaido Prefecture Authorities.

CONCURRENT OCCURRENCE OF EARTHQUAKE AND TYPHOON

Figure 3 shows the earthquake mainshock (M6.6), and its numerous aftershocks within one month after the mainshock (Figure 3a) along with the track and timing of the Super Typhoon Jebi (Figure 3b). Note that here only aftershocks with magnitude above M4 are shown. The area was hit by 47 earthquakes with M≥4 within one month following the mainshock (Figure 3a). The timing of the typhoon shows that Jebi arrived in the earthquake epicentral area and the dam location around 7 pm on 4th September 2018, approximately 23 hours before the mainshock M6.6 (Figure 3a). Therefore, the area was wet and possibly the soil was saturated at the time of the mainshock and aftershocks. It is challenging to separate the contributions of the earthquake and the typhoon to the occurrence of over 6,000 landslides in the region. However, it is possible to state that the simultaneous incidence of these two extreme natural hazards exacerbated the individual destructive impacts of each.

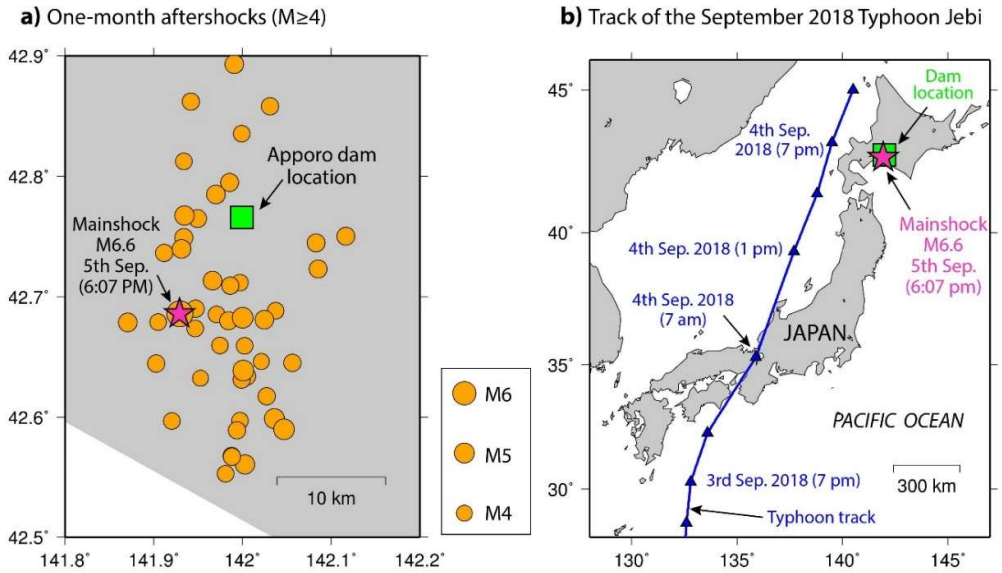

Figure 3. a): The mainshock (M6.6) and one-month aftershocks in the region. **b):** The track of the Super Typhoon Jebi and its timing.

FIELD SURVEY RESULTS

First, we start by looking at the reservoir water level before and after the earthquake as shown in Figure 4. It can be seen that the reservoir water level rose by 30cm within approximately one hour after the earthquake. This is mostly attributed to the intrusion of landslide materials into the reservoir (Figure 4b). Based on our fieldwork in the area and conversations with site engineers, we have witnessed several landslides in the reservoir, some of which were very close to the dam body (Figures 1 and 4). Site engineers guided us to the location of damage to revetments at reservoir banks where we recorded damage details and measured wave runup (Figure 5). The damage shown in Figure 5b was non-existent before the earthquake as confirmed through conversations held with site engineers. Several landslides were easily visible around the damage location (Figure 5b). The runup (R in Figure 2) was measured as $R = 5.3$m (Figure 5a) considering the reservoir water level at the time of the earthquake.

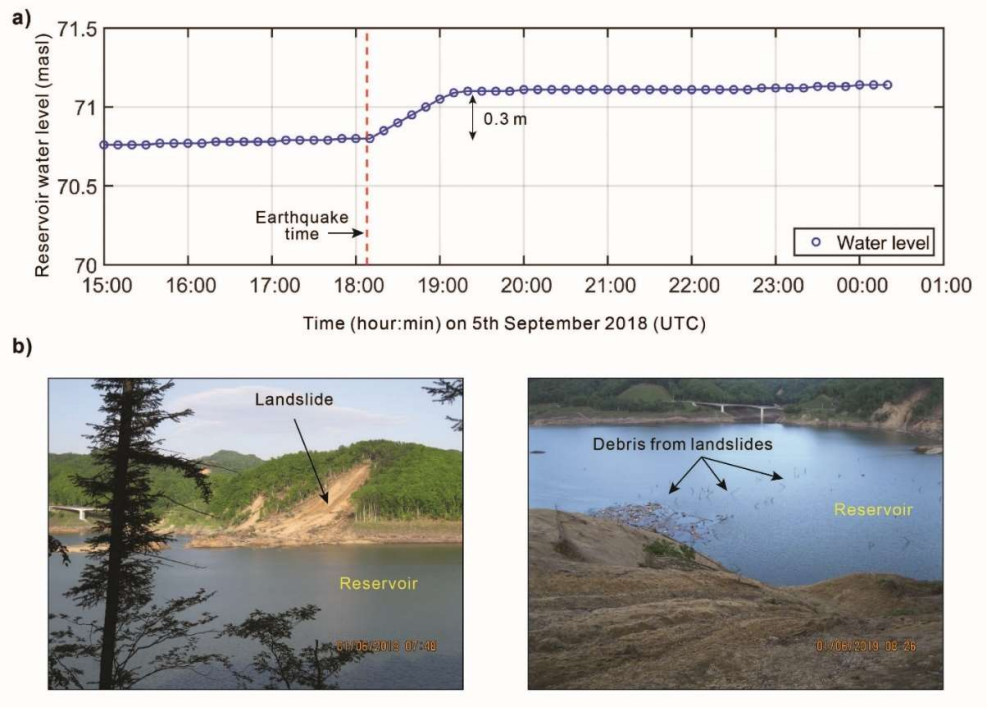

Figure 4. a): Reservoir water level before and after the earthquake. **b):** Photos showing the intrusion of landslide materials into the reservoir.

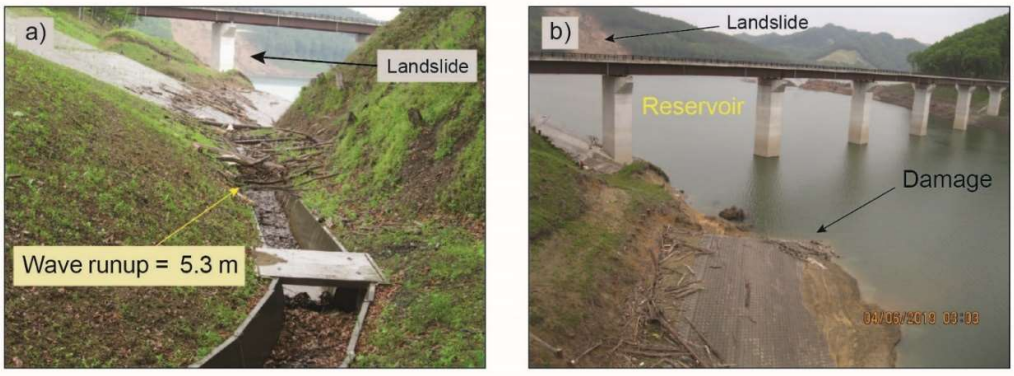

Figure 5. a): Surveyed wave runup point in the banks of the reservoir due to the landslide-generated waves. **b):** A photo showing damage due to the landslide-generated waves.

MODELLING SLOPE STABILITY

Figure 6 presents the slope displacements at the failure state after 200 s of ground earthquake shaking. This analysis was conducted assuming that the groundwater level was at the ground surface after the long-term rainfall. The numerical result indicates that major failure occurred within the topsoil at the middle to upper section of the slope, above the reservoir water level. The shallow nature of the slope failures (Figure 6) is consistent with field observations reported by Heidarzadeh et al. (2023).

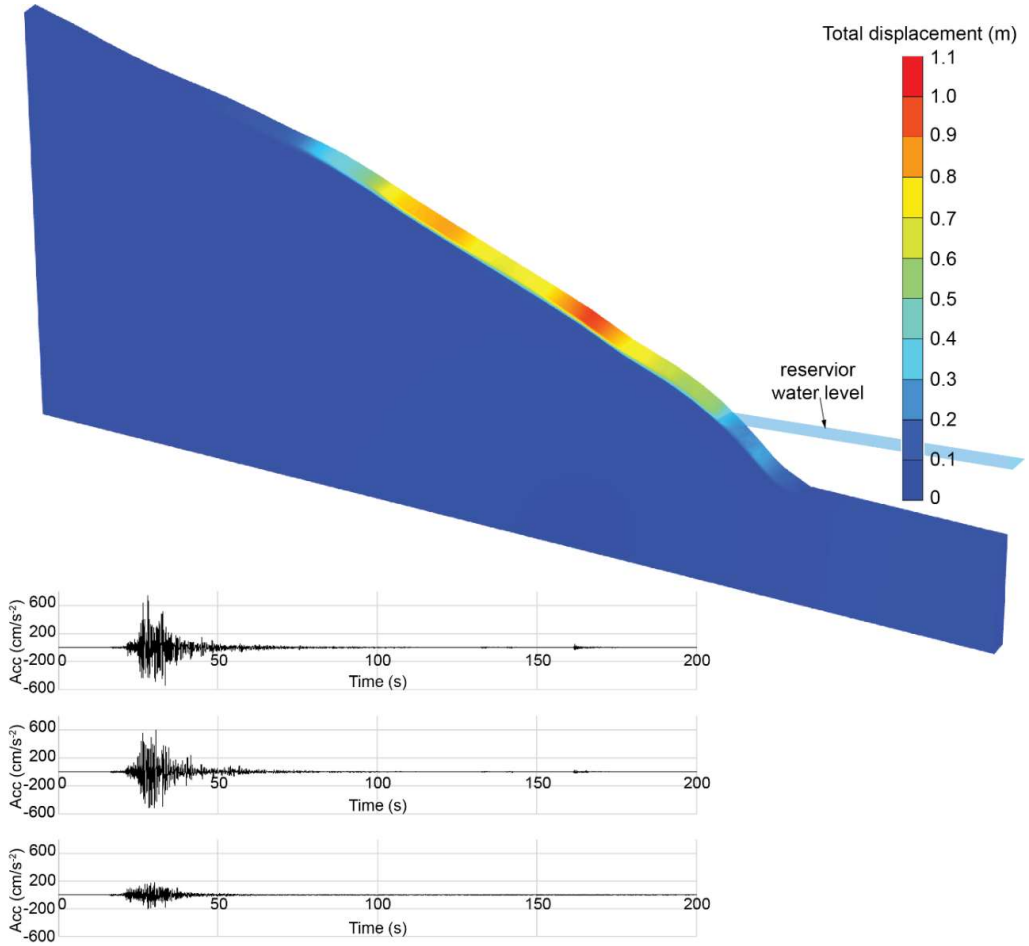

Figure 6. Simulated slope stability analysis of the slopes facing the Apporo dam reservoir using Plaxis 3D. The slope elevation profile was obtained from Google Earth. The ground water level is assumed to be at the ground surface after the long-term rainfall. The earthquake signals were recorded at the Mukawa station (42.7609N, 142.1344E), 11.4 km away from the dam. "Acc" is an abbreviation for "Acceleration".

PREDICTING THE WAVE RUNUP USING EMPIRICAL EQUATIONS

Table 1 contains the parameters for landslide 3 from Heidarzadeh et al. (2023). A slide porosity n = 40% has been assumed and the wave propagation angle g (Figure 2) is estimated as 17°. The spreadsheet (step 1) of Evers et al. (2019) is shown in Figure 7 which predicts a maximum wave amplitude of 12.9m (a0,c1 in Figure 7) and a maximum height of 27.7m in the impact zone (a0,c1 + a0,t1). The waves decay over the distance r = 650m to an amplitude of 1.2m (ac1) and a wave height of 2.7m (ac1 + at1) offshore the runup location. The

corresponding runup height (not shown in Figure 7) is 6.5m, which is 23% larger than 5.3m observed in the field.

Table 1. Parameters for landslide 3 from Heidarzadeh et al. (2023) for wave generation, propagation and runup at the shore and at the dam for the Apporo dam incident. Here, $V_s = [2gDz(1 - \tan d \cot a)]^{1/2}$ from Evers et al. (2019) and the slide porosity is assumed as n = 40%.

Parameter	Value	Parameter	Value
Slide impact angle α (°)	20	Shore: Radial distance r (m)	650
Vertical drop height Δz (m)	85	Shore: Wave propagation angle γ (°)	17
Dynamic bed friction angle δ (°)	12	Shore: Still water depth h (m)	27
Slide impact velocity V_s (m/s)	26	Shore: Runup angle β (°)	10
Slide width b_s (m)	140	Shore: Observed runup height R (m)	5.3
Maximum slide thickness s (m)	2.5	Dam: Radial distance r (m)	680
Bulk slide volume $\forall_s$ (m^3)	71400	Dam: Wave propagation angle γ (°)	60
Bulk slide density ρ_s (kg/m^3)	1700	Dam: Still water depth h (m)	27
Slide porosity n (%)	40	Dam: Runup angle β (°)	51
Still water depth h (m)	27	Dam: Freeboard f (m)	20.4

Generation | Propagation (3D)
Project: Proceeding Heidarzadeh et al. (2024)

Governing parameters			
Wave generation			
Slide impact velocity	V_s	26	[m/s]
Bulk slide volume	$\forall_s$	71400	[m^3]
Slide thickness	s	2.5	[m]
Slide width	b	140	[m]
Bulk slide density	ρ_s	1700	[kg/m^3]
Bulk slide porosity	n	40	[%]
Slide impact angle	α	20	[°]
Still water depth	h	27	[m]
Wave propagation			
Radial distance	r	650	[m]
Wave propagation angle	γ	17	[°]

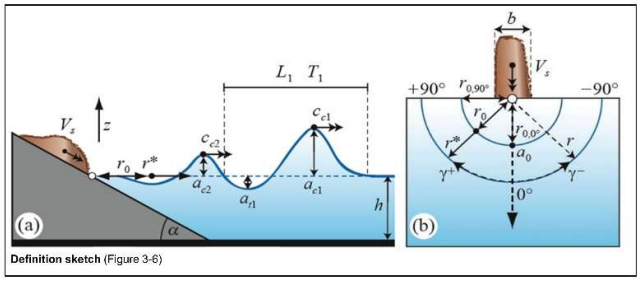

Definition sketch (Figure 3-6)

Main results				
Impact radius for γ = 0°	$r_{0,0°}$	Eq. (3.22)	85	[m]
Impact radius for γ = 90°	$r_{0,90°}$	Eq. (3.23)	104	[m]
Impact radius	$r_0(\gamma)$	Eq. (3.24)	86	[m]
Surrogate radial distance	r^*	Eq. (3.25)	564	[m]
Initial first wave crest amplitude	$a_{0,c1}$	Eq. (3.26)	12.9	[m]
Initial first wave trough amplitude	$a_{0,t1}$	Eq. (3.27)	14.8	[m]
Initial second wave crest amplitude	$a_{0,c2}$	Eq. (3.28)	4.7	[m]
First wave crest amplitude	a_{c1}	Eq. (3.29)	1.2	[m]
First wave trough amplitude	a_{t1}	Eq. (3.30)	1.5	[m]
Second wave crest amplitude	a_{c2}	Eq. (3.31)	2.0	[m]
First wave crest celerity	c_{c1}	Eq. (3.32)	15.8	[m/s]
Second wave crest celerity	c_{c2}	Eq. (3.33)	11.8	[m/s]
Wave period (first wave)	T_1	Eq. (3.34)	27.8	[s]
Wave length (first wave)	L_1	Eq. (3.35)	440	[m]

Limitations (Table 3-3)			
Slide Froude number	$0.40 \le F \le 3.40$	1.60	[-]
Relative slide thickness	$0.15 \le S \le 0.60$	0.09	[-]
Relative slide mass	$0.25 \le M \le 1.00$	1.19	[-]
Relative slide density	$0.59 \le D \le 1.72$	1.70	[-] (1)
Relative granulate density	$0.96 \le \rho_g/\rho_w \le 2.75$	2.83	[-] (1)
Relative slide volume	$0.187 \le V \le 0.750$	0.70	[-]
Bulk slide porosity	$30.7 \le n \le 43.3$	40	[%] (1)
Slide impact angle	$30° \le \alpha \le 90°$	20	[°]
Relative slide width	$0.83 \le B \le 5.00$	5.19	[-]
Relative radial distance	$1 \le r/h \le 16$	24.07	[-]
Wave propagation angle	$-90° \le \gamma \le 90°$	17	[°]
Impulse product parameter	$0.13 \le P \le 2.08$	0.50	[-]

(1) extended density range $0.59 \le D \le 1.72$

Figure 7. Spreadsheet "Generation | Propagation (3D)" of Evers et al. (2019) with the input parameters from Table 1 (orange), satisfied (green) and not satisfied (pink) limitations and main results. For details about this empirical approach, see Evers et al. (2019) and the accompanied spreadsheet at: https://zenodo.org/record/3492000#.XmAQwW52uas.

Nevertheless, this 23% discrepancy in step 1 can be considered acceptable given that the empirical equations in Evers et al. (2019) are based on idealised conditions including mesh-packed granular slides in the 3D approach, and constant slide impact and wave runup slopes. Note also that the wave amplitude at the base of the shore slope (approximately in the centre

of the reservoir) is used to calculate the runup height with a 2D runup equation, i.e. whilst the amplitude decay due to lateral energy spread is taken into account up to this base, it is neglected on the slope itself. Further, six of the 12 parameter limitations of the empirical equations for wave generation and propagation are not satisfied (Figure 7) whilst all four for the runup are satisfied (not shown in Figure 7). There are uncertainties regarding the slide parameters and water depth too. The effects of wave parameters due to deviations of these idealisations are not covered in step 1 of the spreadsheet developed by Evers et al. (2019). However, they are described and quantified in step 2 (Evers et al. 2019), which can be important.

At the dam centre, the spreadsheet of Evers et al. (2019) predicts R = 2.6m for the parameters given in Table 1. Note that there are no corresponding observations from the field for the dam centre. This runup is significantly smaller than the freeboard of 20.4m (at the time of the earthquake) such that there was no immediate danger for the downstream population. Given that the method of Evers et al. (2019) provides only preliminary estimates, it is strongly recommended to conduct a comprehensive, prototype-specific numerical or scaled laboratory study if the predicted R at the dam is close to the dam's freeboard.

HAZARDS IMPLICATIONS FOR THE UK

In the UK, the highest risk of landslide-induced waves on reservoirs would appear to be in steep V-shaped valleys, with higher-than-average rainfall and seismic risk. The mountainous regions of Wales and Scotland meet these criteria, and indeed Wales has had several examples of major landslide tragedies (on coal waste tips) in the past. Whilst major earthquakes are rare in the UK, the highest seismicity levels are shown in standard guidance (Figure 5 of Charles et al. 1991) as mid/northwest England, Wales, and north-west Scotland; areas where rainfall is also high.

Figure 8 shows an initial estimation of the areas of the UK most susceptible to landslide risk to reservoirs, using GIS layers for elevation, rainfall, and seismicity. Comparing the highest risk zone (Region 3, in Figure 8) with the coordinates of all reservoirs on the public registers (as of May 2024), shows that some 38 large-raised reservoirs in England, 111 reservoirs in Wales and 103 controlled reservoirs in Scotland fall within this highest risk zone. This initial analysis of landslide risk to UK reservoirs indicates that less than 10% of large reservoirs on the registers may need to have this risk included when undertaking a quantitative risk assessment of potential failure modes. Panel engineers undertaking inspections of dams in these higher risk areas should be extra vigilant of reservoir rim stability indicators when undertaking their visits.

CONCLUSIONS

In this article, we highlighted the hazards and risks from landslide-generated waves in dam reservoirs by reporting, analysing and modelling an incident that occurred in Apporo dam reservoir in Japan in September 2018. Main findings are:

- By field surveys, we measured a runup height of 5.3m at a location in the reservoir banks.
- The empirical model of Evers et al. (2019) was applied to replicate the runup which successfully predicted the observed runup with an acceptable discrepancy of 23%.
- Numerical modelling using Plaxis 3D revealed that the slopes were fully saturated before the earthquake, and earthquake shaking triggered the landslide.

Managing Risks for Dams and Reservoirs

- We found that fewer than 10% of large UK reservoirs may need to include landslide risk in their failure mode assessments. Panel engineers should be especially vigilant regarding reservoir rim stability during inspections in higher risk areas (Regions 2 and 3, in Figure 8).
- To conduct preliminary quantitative assessments of the potential for landslide-generated waves in UK dam reservoirs, we recommend the following four steps:

i) **Step 1:** Investigate whether the reservoir is located within the 'Regions 2 and 3' of our Figure 8 or not.

ii) **Step 2:** If the answer to Step 1 is positive, conduct numerical modelling of landslides and assess Factor of Safety (FoS) of the slopes and estimate displacements (Figure 6).

iii) **Step 3:** If there is a potential for failure (e.g., FoS < 1.2), apply the approach of Evers et al. (2019) to estimate the amplitudes of the landslide-generated waves (Figure 7).

iv) **Step 4:** For cases where the estimated wave amplitudes are close to the dam freeboard, consider appropriate remedy/resilience measures.

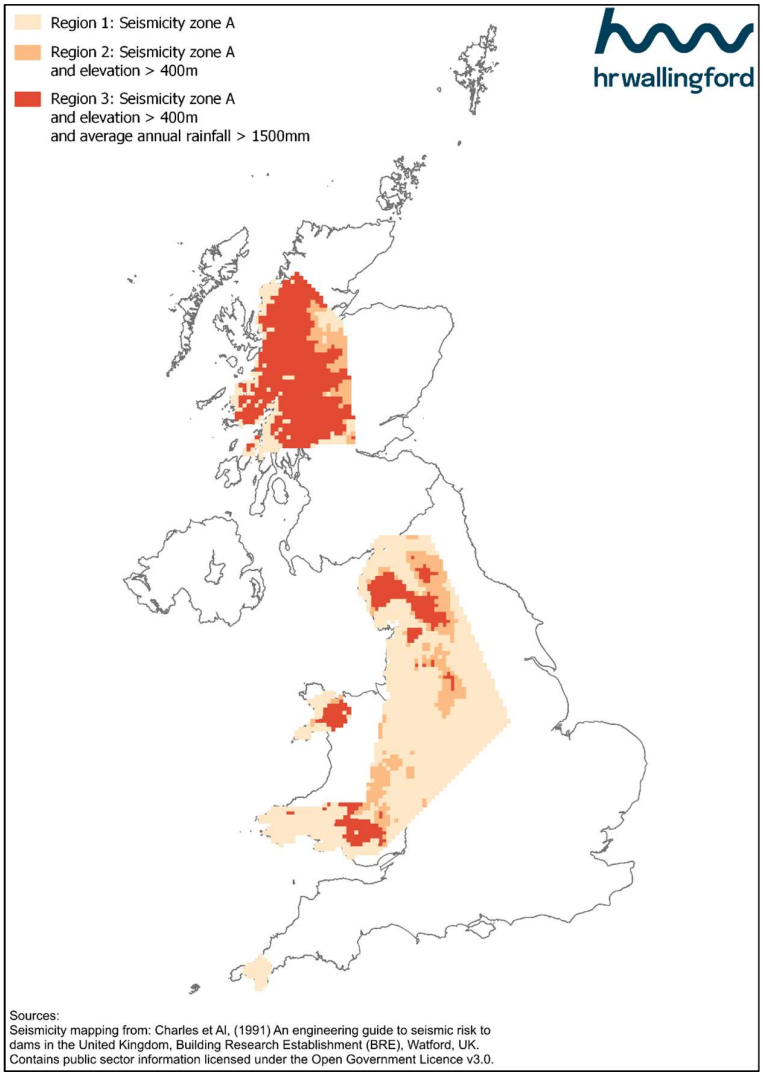

Figure 8. Areas of elevated risk of landslide into reservoirs in the UK based on available GIS data on elevation, rainfall, and seismicity.

REFERENCES

Acford M (2015). The reservoirs act 1975 and reservoir risk designations. *Dams and Reservoirs*, 25(2), 56-57. https://doi.org/10.1680/jdare.15.00025.

Aimaiti Y, Liu W, Yamazaki F, Maruyama Y (2019). Earthquake-induced landslide mapping for the 2018 Hokkaido Eastern Iburi Earthquake Using PALSAR-2 data. *Remote Sensing*, 11(20), 2351. https://www.mdpi.com/2072-4292/11/20/2351.

Biot MA (1956). General solutions of the equations of elasticity and consolidation for a porous material. *Journal of Applied Mechanics*, 23(2), 91-96. https://doi.org/10.1115/1.4011213.

Charles JA, Abbiss CP, Gosschalk EM, Hinks JL (1991). An engineering guide to seismic risk to dams in the United Kingdom, Building Research Establishment (BRE), Watford, UK.

Ersoy H, Karahan M, Gelisli K, Akgun A, Anilan T, Sunnetci MO, Yahsi BK (2019). Modelling of the landslide-induced impulse waves in the Artvin Dam reservoir by empirical approach and 3D numerical simulation. *Engineering Geology*, 249(1), 112-128. https://doi.org/10.1016/j.enggeo.2018.12.025.

Evers FM, Heller V, Fuchs H, Hager WH, Boes RM (2019). Landslide generated impulse waves in reservoirs - Basics and computation, 2nd edition. ETH Zurich, Zurich. https://vaw.ethz.ch/en/the-institute/publications/vaw-communications/2010-2019.html, https://zenodo.org/record/3492000#.XmAQwW52uas (spreadsheet).

Fuchs H, Boes R (2010). Berechnung felsrutschinduzierter Impulswellen im Vierwaldstättersee. *Wasser Energie Luft*, 102 (3), 215-221 (in German). https://doi.org/10.3929/ethz-b-000256996.

Gabl R, Seibl J, Gems B, Aufleger M (2015). 3-D-numerical approach to simulate the overtopping volume caused by an impulse wave comparable to avalanche impact in a reservoir. *Natural Hazards and Earth System Sciences*, 15(12), 2617-2630. https://doi.org/10.5194/nhess-15-2617-2015.

Heidarzadeh M, Miyazaki H, Ishibe T, Takagi H, Sabeti R (2023). Field surveys of September 2018 landslide-generated waves in the Apporo dam reservoir, Japan: Combined hazard from the concurrent occurrences of a typhoon and an earthquake. *Landslides*, 20, 143-156. https://doi.org/10.1007/s10346-022-01959-8.

Heller V, Hager WH (2010). Impulse product parameter in landslide generated impulse waves. *Journal of Waterway, Port, Coastal, and Ocean Engineering*, 136(3), 145-155. http://dx.doi.org/10.1061/(ASCE)WW.1943-5460.0000037.

Heller V, Hager WH, Minor H-E (2009). Landslide generated impulse waves in reservoirs - Basics and computation. ETH Zurich, Zurich. https://vaw.ethz.ch/en/the-institute/publications/vaw-communications/2000-2009.html.

Heller V, Ruffini G (2023). A critical review about generic subaerial landslide-tsunami experiments and options for a needed step change. *Earth-Science Reviews*, 242, 104459. https://doi.org/10.1016/j.earscirev.2023.104459.

Huang B, Yin Y, Liu G, Wang S, Chen X, Huo Z (2012). Analysis of waves generated by Gongjiafang landslide in Wu Gorge, Three Gorges Reservoir, on November 23, 2008. *Landslides*, 9(3), 395-405. https://doi.org/10.1007/s10346-012-0331-y.

Managing Risks for Dams and Reservoirs

Huang B, Yin Y, Li R, Zhang P, Qin Z, Li Y, Cheng S, Li Q, Xu K (2023). Three-dimensional experimental investigation on hazard reduction of landslide-generated impulse waves in the Baihetan Reservoir, China. *Landslides*, 20, 2017-2028. https://doi.org/10.1007/s10346-023-02068-w.

Itsukushima R (2023). Historical development and the present status of Japanese dams. *River Research and Applications*, 39(6), 1136-1147. https://doi.org/10.1002/rra.4129.

Japan Commission on Large Dams (2018). Dams in Japan: overview 2018. Online materials at: https://jcold.or.jp/cm/wp-content/uploads/2020/01/Dams-in-Japan-2018-web%E7%94%A8.pdf (accessed on 9th May 2024).

Macdonald A (2011). Reservoir safety in Scotland–The Reservoirs (Scotland) Bill–an overview. *Dams and Reservoirs*, 21(1), 9-13. https://doi.org/10.1680/dare.2011.21.1.9.

MacFarlane DF, Jenks DG (1996). Stabilisation and performance of No. 5 Creek Slide, Clyde Power Project, New Zealand. Proc. 7th International Symposium *Landslides* Trondheim 3, 1739-1746. Senneset, K. ed. Balkema, Rotterdam.

Müller L (1964). The rock slide in the Vajont Valley. *Rock Mechanics and Engineering Geology*, 2(3-4), 148-212.

Sasaki T, Kondo M (2018). Trends in dam upgrading in Japan. *Journal of Disaster Research*, 13(4), 585-594. https://doi.org/10.20965/jdr.2018.p0585.

Sattar A, Goswami A, Kulkarni AV, Emmer A, Haritashya UK, Allen S, Frey H, Huggel C (2021). Future glacial lake outburst flood (GLOF) hazard of the South Lhonak Lake, Sikkim Himalaya. *Geomorphology*, 388(9), 107783. https://doi.org/10.1016/j.geomorph.2021.107783.

Xiao L, Wang J, Ward SN, Chen L (2018). Numerical modeling of the June 24, 2015, Hongyanzi landslide generated impulse waves in Three Gorges Reservoir, China. *Landslides*, 15 (12), 2385-2398. https://doi.org/10.1007/s10346-018-1057-2.

Yamagishi H, Yamazaki F (2018). Landslides by the 2018 Hokkaido Iburi-Tobu Earthquake on September 6. *Landslides*, 15(12), 2521-2524. https://doi.org/10.1007/s10346-018-1092-z.

Yin Y-P, Huang B, Chen X, Liu G, Wang S (2015). Numerical analysis on wave generated by the Qianjiangping landslide in Three Gorges Reservoir, China. *Landslides*, 12 (2), 355-364. https://doi.org/10.1007/s10346-015-0564-7.

Zhang S, Li R, Wang F, Lio A (2019). Characteristics of landslides triggered by the 2018 Hokkaido Eastern Iburi earthquake, northern Japan. *Landslides*, 16(9), 1691-1708. https://doi.org/10.1007/s10346-019-01207-6.